NANO LETTERS

Letter

pubs.acs.org/NanoLett

Hot-Electron Intraband Luminescence from GaAs Nanospheres Mediated by Magnetic Dipole Resonances

Jin Xiang,[†] Shuai Jiang,[†] Jingdong Chen,[†] Jinxiang Li,[†] Qiaofeng Dai,[†] Chengyun Zhang,[†,‡] Yi Xu,[§] Shaolong Tie,[∥] and Sheng Lan*[,†]

[†]Guangdong Provincial Key Laboratory of Nanophotonic Functional Materials and Devices, School of Information and Optoelectronic Science and Engineering, [∥]School of Chemistry and Environment, South China Normal University, Guangzhou 510006, China

[‡]School of Physics and Electronic Engineering, Guangzhou University, Guangzhou 510006, China

[§]Department of Electronic Engineering, College of Information Science and Technology, Jinan University, Guangzhou 510632, China

S *Supporting Information*

ABSTRACT: Significantly enhanced electric field in plasmonic hot spots can dramatically increase the linear and nonlinear absorption of light, leading to a high-temperature electron gas which radiates, through mainly intraband transition, a broadband luminescence quite similar to blackbody radiation. Here, we demonstrate that such hot-electron intraband luminescence (HEIL) can also be achieved by exploiting the significantly enhanced electric field at the magnetic dipole resonances of gallium arsenide (GaAs) nanospheres (NSs). We show that monocrystalline GaAs NSs with distinct electric and magnetic dipole (ED and MD) resonances can be obtained by using femtosecond laser ablation and annealing. Significantly enhanced second harmonic generation and broadband HEIL are observed when the MD resonances of such GaAs NSs are resonantly excited. The lifetime of the HEIL is found to be as short as ~82 ps, indicating a significant enhancement in radiative intraband transition rate. We reveal that the slope extracted from the dependence of the HEIL intensity on the irradiance is linearly proportional to the energy of the emitted photon. The existence of distinct ED and MD resonances in combination with a direct bandgap makes GaAs NSs an attractive candidate for constructing novel all-dielectric metamaterials and active photonic devices.

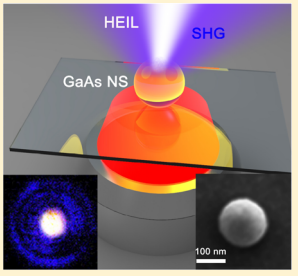

KEYWORDS: *GaAs nanosphere, hot-electron intraband luminescence, second harmonic generation, magnetic dipole resonance, femtosecond laser ablation and annealing*

Plasmonic hot spots, in which the electric field is greatly enhanced, have been the focus of numerous studies because they are not only interesting for fundamental research but also important for practical application.[1,2] Typical hot spots usually appear at the tips of metallic nanoparticles or the nanogaps between two metallic nanoparticles. The significantly enhanced electric field in hot spots has been widely utilized to enhance the linear and especially the nonlinear optical responses of nanomaterials, such as Raman scattering, second harmonic generation (SHG), and two-photon-induced luminescence (TPL), and so forth.[3,4] Early in 2000, it was found that gold nanorods can emit very strong photoluminescence due to the existence of longitudinal surface plasmon resonances.[5] The TPL of gold nanorods has received intensive and extensive studies because of its potential applications in sensing, bioimaging, and optical data storage.[6−8] However, the physical mechanism for the TPL of gold nanorods remains controversial. Although a slope close to 2.0 is generally observed in the dependence of the TPL intensity on the irradiance plotted in a double-logarithmic coordinate, it is still debated whether the transition of electrons from the d band to the sp conduction band is induced by simultaneously or sequentially absorbing two photons.[9,10] Very recently, a new physical mechanism was proposed, in which the photoluminescence from plasmonic hot spots is attributed to the intraband transition of hot electrons.[11] It was revealed by a detailed analysis that the slope extracted from the luminescence intensity as a function of the irradiance is linearly proportional to the energy of emitted photon, which is a characteristic of hot-electron intraband luminescence (HEIL). This behavior is observed only for single hot spots, and it disappears if a large number of hot spots is characterized.[11,12] The HEIL observed on the surfaces of rough silver (Ag) or gold (Au) film appears as broadband, including not only the up-converted part with photon energies larger than that of the excitation laser but also the down-converted one with photon energies smaller than the bandgap energy of Ag or Au. It was suggested that the HEIL originates from the high-temperature electron gas induced by femtosecond (fs) laser pulses and the significantly enhanced electric field in hot spots plays a crucial role in generating the high-temperature electron gas.[11]

Received: April 24, 2017
Revised: June 29, 2017
Published: July 10, 2017

DOI: 10.1021/acs.nanolett.7b01724
Nano Lett. XXXX, XXX, XXX−XXX

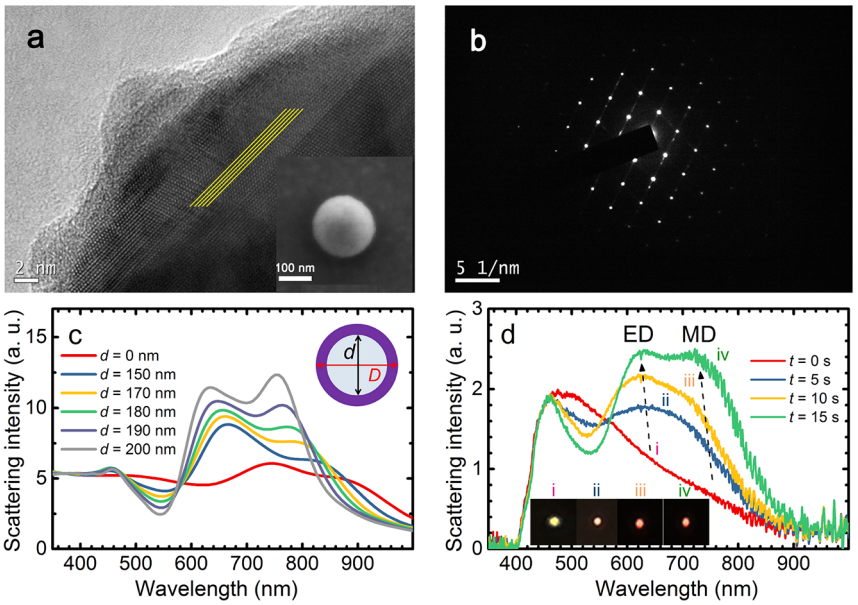

Figure 1. Phase transition from amorphous GaAs (a-GaAs) to crystalline GaAs (c-GaAs) induced by fs laser annealing. (a) TEM image of a GaAs NS after annealing. The SEM image is shown in the inset. (b) Electron diffraction pattern of a GaAs NS after annealing. (c) Evolution of the scattering spectrum of a core(c-GaAs)−shell(a-GaAs) NS with an increasing core diameter simulated by using the FDTD method. (d) Evolution of the scattering spectrum of a fabricated GaAs NS with increasing irradiation time by using fs laser pulses with a wavelength of 780 nm and an irradiance of 0.13 mJ/cm^2. The change of the scattering light color during the annealing process is shown in the insets.

Although efficient HEIL can be generated by plasmonic hot spots formed by metallic nanoparticles or nanostructures,[11,13] such hot spots may disappear at high temperatures because of the melting or deformation of metallic nanoparticles/nanostructures. For example, the quench of the TPL of gold nanorods, which is caused by the transformation of gold nanorods into gold nanospheres after the irradiation of high-energy fs laser pulses, has been successfully exploited to realize multidimensional optical data storage.[7] For this reason, much effort has been devoted to metal−dielectric hybrid nanostructures, in which the plasmonic effect is only employed to enhance the electric field in dielectric materials.[14,15] Lasing of semiconductor nanowires placed on a thin Ag film and hot luminescence from silicon (Si) nanowires coated with Ag films have been successfully demonstrated.[13−15] In these cases, heat generation and temperature rise occur mainly in semiconductors which possess much higher melting points than metals. In recent years, all-dielectric metamaterials have attracted great interest because metal-based metamaterials fail to work at optical frequencies owing to large ohmic loss. It has been found that dielectric nanoparticles with large permittivity, such as Si,[16−19] germanium (Ge),[20] tellurium (Te),[21] and gallium arsenide (GaAs),[22] which exhibit distinct electric dipole (ED) and magnetic dipole (MD) resonances in the visible to near-infrared spectral range, act as promising building blocks for all-dielectric metamaterials.[23−25] Since Si nanospheres (NSs) with diameters in the range of 150−250 nm exhibit strong MD resonances in the visible to near-infrared spectral range, the fabrication and characterization of Si NSs have received intensive and extensive studies in recent years.[26−28] Apart from the linear optical properties of Si nanoparticles, much attention has been paid to their nonlinear optical responses, such as the enhanced harmonic generation, ultrafast all-optical switching, and multiphoton-induced luminescence, realized by exploiting their ED/MD resonances.[29−32] However, it is well-known that Si is not suitable for making good emitters because of its indirect bandgap. In addition, two-photon-induced absorption (TPA) or even three-photon-induced absorption is necessary to generate high-density hot electrons in the conduction band of Si because of the large bandgap (~3.4 eV) at the Γ point. As compared with Si nanoparticles, less attention has been paid to GaAs nanoparticles because of the difficulty in fabrication. Similar to the directional scattering observed in Si NSs, zero backward scattering at the wavelength satisfying the first Kerker's condition was also demonstrated on an array of GaAs nanopillars.[33] Moreover, the resonances in GaAs/AlGaAs-based metasurfaces have also been exploited to enhance SHG and realize ultrafast tuning of surface reflectance.[34−36]

In this Letter, we demonstrate that efficient HEIL can be generated by resonantly exciting the MD resonances of monocrystalline GaAs NSs which can be fabricated by using fs laser ablation and annealing. The existence of distinct ED and MD resonances in combination with a direct bandgap makes GaAs NSs an attractive candidate for constructing novel all-dielectric metamaterials and active photonic devices.

Results and Discussion. *Fabrication of Monocrystalline GaAs NSs with Distinct ED and MD Resonances.* So far, the most popular, cheap, and convenient technique used to fabricate semiconductor nanoparticles is fs laser ablation because lithographic methods are more complex and do not allow the fabrication of spherical nanoparticles. Actually, it has been successfully employed to obtain single Si NSs of various sizes and regular arrays of Si NSs.[16−18,26,27] As compared with lithographic methods in which many nonradiative recombination centers will be introduced, nanoparticles fabricated by fs laser ablation are more suitable for studying HEIL and making good emitters. To the best of our knowledge, however, it remains a big challenge to fabricate high-quality GaAs NSs, which exhibit distinct MDs and ED resonances, by using fs laser ablation. From the technological point of view, it is quite difficult to obtain GaAs nanoparticles with a spherical shape

DOI: 10.1021/acs.nanolett.7b01724
Nano Lett. XXXX, XXX, XXX−XXX

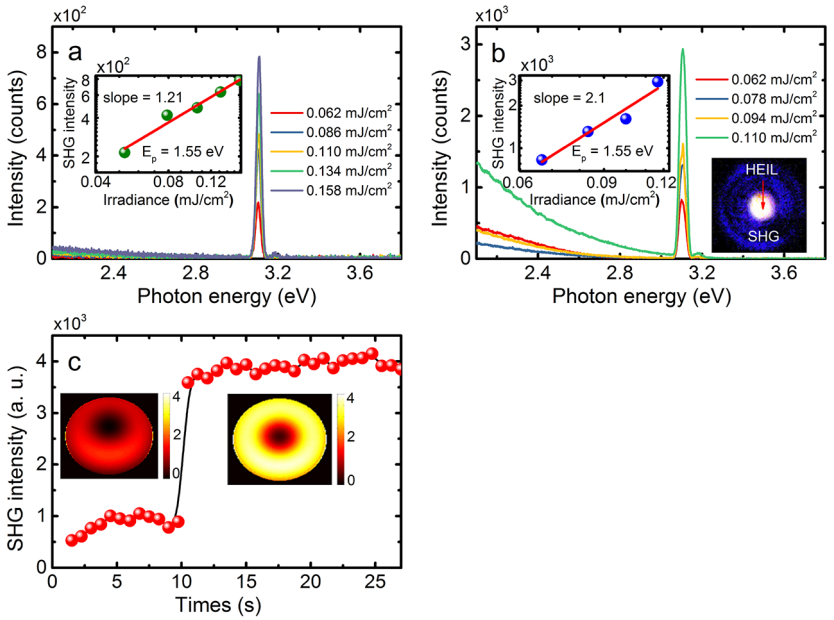

Figure 2. Nonlinear optical properties of GaAs NSs. Nonlinear response spectra of a fabricated GaAs NS with $D \sim 190$ nm before (a) and after (b) annealing measured at different irradiances. In each case, the dependence of the SHG intensity on the irradiance is shown in the inset. The photon energy of the excitation laser light is $E_p = 1.55$ eV. The emission pattern of the GaAs NS after annealing is shown in the inset of panel b. (c) Dependence of the SHG intensity of a GaAs NS on the annealing time. The electric field distributions simulated for an a-GaAs NS and a c-GaAs NS with $D = 200$ nm are shown in the insets.

and correct stoichiometric ratio. In addition, GaAs nanoparticles obtained under the nonequilibrium condition in fs laser ablation are generally polycrystalline or even amorphous, making it difficult to observe MD resonances.

By employing a laser-induced backward transfer technique,[26,27] we have successfully fabricated GaAs NSs with different diameters (see Supporting Information, SI, S1). The morphology of the as-prepared GaAs NSs was examined by using scanning electron microscopy (SEM), while the crystal structure was characterized by transmission electron microscopy (TEM) (see SI S2 and S3). On the basis of the TEM images and electron diffraction patterns, it was found that the GaAs NSs are generally polycrystalline or even amorphous. Fortunately, monocrystalline GaAs NSs can be achieved by annealing with fs laser pulses of a high repetition rate of 76 MHz (see SI S3, S4, and S5). In Figure1a,b, we show the SEM and TEM images and electron diffraction pattern of a typical GaAs NS after annealing. Although a very thin amorphous shell was still observed, it was confirmed that the core of the GaAs NS was monocrystalline.

Actually, the phase transition of the GaAs NS from amorphous to monocrystalline was also clearly reflected in the scattering spectrum of the GaAs NS. To find out the effects of crystal structure on the scattering properties of GaAs NSs, we have simulated the evolution of the scattering spectrum of a GaAs NS with a core (monocrystalline)−shell (amorphous) structure when the core diameter is increased, as shown in Figure 1c. The total diameter of the GaAs NS was fixed at $D = 200$ nm. The scattering spectra were calculated by using the finite-difference time-domain (FDTD) method based on the complex refractive indices of crystalline GaAs (c-GaAs) and amorphous GaAs (a-GaAs)[37,38] (see SI S6). For an a-GaAs NS with $D = 200$ nm (i.e., $d = 0$ nm), a broad and weak scattering peak is observed at ∼750 nm owing to the large imaginary part of the complex refractive index of a-GaAs. As the core diameter is increased to $d = 150$ nm, the scattering peak is blue-shifted to ∼660 nm, while the scattering intensity is enhanced by a factor of ∼1.6. In addition, a small shoulder appears at ∼840 nm. As the core diameter is further increased, one can see a slow increase of the main-peak intensity and a rapid increase of the small-shoulder intensity. In addition, a continuous blueshift is observed for both the main peak and the small shoulder. When the core diameter is increased to $d = 190$ nm (i.e., the thickness of the shell is reduced to 5 nm), the intensities of the two peaks become almost the same. For a c-GaAs NS, the scattering spectrum is dominated by the peak at the longer wavelength which corresponds to the MD resonance. On the basis of the simulation results, we can conclude that the crystal structure plays a crucial role in determining the scattering properties of GaAs NSs. It is the phase transition of the crystal structure from amorphous to crystalline that leads to the appearance of distinct MD and ED resonances in the scattering spectra. As compared with the Si NS, the line widths of the ED and MD resonances of the GaAs NS with the same diameter ($d = 200$ nm) are slightly broadened owing to the larger imaginary part of the complex refractive index (see SI S7). As a result, a larger overlap between the MD and ED resonances is observed for the GaAs NS, implying a stronger coherent interaction between them.

In experiments, the evolution of the scattering spectrum of the GaAs NS is shown in Figure 1d. Before annealing, only a scattering peak at ∼470 nm was observed. After the first annealing of 5 s, a new scattering peak with nearly the same intensity as the original one emerged at ∼630 nm. It can be seen that the intensity of the new peak at ∼620 nm exceeded that of the original one at ∼470 nm after the second annealing of 5 s. In addition, a small shoulder began to appear at ∼730 nm. With the third annealing of 5 s, the small shoulder evolved into a new peak which possesses the same intensity with that at ∼620 nm. As can be seen, the evolution of the scattering

DOI: 10.1021/acs.nanolett.7b01724
Nano Lett. XXXX, XXX, XXX−XXX

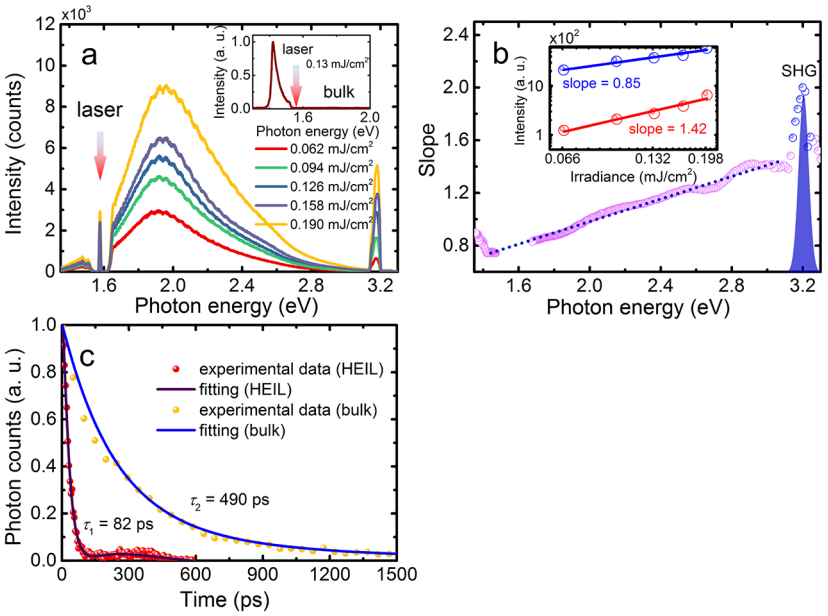

Figure 3. HEIL from resonantly excited c-GaAs NSs. (a) Evolution of the HEIL spectrum of a c-GaAs NS with $D \sim 190$ nm with increasing irradiance. The photoluminescence spectrum of bulk GaAs excited under the same condition is shown in the inset. (b) Dependence of the extracted slope on the photon energy observed for the HEIL of the GaAs NS. The dependence of the HEIL intensity on the irradiance plotted for two photon energies of 1.72 and 3.1 eV in a double-logarithmic coordinate are shown in the inset. (c) Decay of the HEIL of a GaAs NS with $D \sim 190$ nm, which is fitted by two exponential decays, after the excitation of fs laser pulses. The decay of the luminescence from bulk GaAs is also provided for comparison. The detection wavelengths for the luminescence lifetime of the GaAs NS and bulk GaAs were chosen to be 550 and 860 nm, respectively.

spectrum observed in the annealing process is in good agreement with that predicated by the numerical simulations (see Figure 1c). Although most of the scattering properties of the GaAs NSs can be modeled by using the simple core−shell structure described above, this physical model is still too simple to account for the complicated structures of the GaAs NSs fabricated by fs laser ablation. As a more complete model, one can consider the GaAs NSs to be a combination of many smaller c-GaAs nanoparticles incorporated in an amorphous matrix. Since small GaAs nanoparticles possess scattering peaks at short wavelengths, one can observe a strong scattering peak at ∼470 nm before annealing. However, the scattering peak will become weak or even negligible after annealing because small c-GaAs nanoparticles aggregate into a larger core (see SI S5).

Efficient HEIL from Monocrystalline GaAs NSs Resonantly Excited at MD Resonances. In fact, the change in crystal structure is also indirectly reflected in the nonlinear optical responses of GaAs NSs excited by fs laser pulses. It has been shown more than 30 years ago by using a-GaAs as an example that the detection of SHG is an extremely powerful tool for studying both the dynamics of laser-induced annealing and the quality of the crystal obtained. In Figure 2a,b, we show the nonlinear response spectra measured for a GaAs NS before and after annealing. In Figure 2a, only very weak SHG, whose intensity depended almost linearly on the irradiance (see the inset of Figure 2a), was observed. It is well-known that the surface of a nanoparticle where the symmetry is broken plays a crucial role in SHG. In addition, it has been demonstrated that a-GaAs has a second-order susceptibility much smaller than c-GaAs.[39−41] Therefore, it is easily understood why the as-prepared GaAs NSs with a-GaAs shells exhibit a very weak SHG. Since the measurements of the nonlinear response spectra were usually accompanied by the annealing of the GaAs NS because of the low threshold for annealing, the slope extracted from the dependence of the SHG intensity on the irradiance exhibited a value smaller than 2.0 (see SI S8). The physical origin is the rapid increase of nonradiative and radiative recombination rates with increasing irradiance during the annealing process. If the measurements of the nonlinear response spectra were intentionally performed under extremely low irradiances, then a slope of ∼2.0 could be observed (see SI S8). In Figure 2b where the nonlinear response spectra of the GaAs after annealing are shown, one can observe not only the enhanced SHG intensity but also a quadratic dependence of the SHG intensity on the irradiance for c-GaAs. More interestingly, broadband up-converted luminescence appeared on the long-wavelength side of the second harmonic, and its intensity increased rapidly with increasing irradiance. In fact, we monitored the SHG intensity of a GaAs NS during the annealing process which indirectly reflects the phase transition in crystal structure, as shown in Figure 2c. For annealing time less than 9 s ($t < 9$ s), the SHG intensity remained nearly unchanged. At $t = 9$ s, a rapid increase in SHG intensity was observed, indicating the phase transition of crystal structure from amorphous/polycrystalline to monocrystalline. The phase transition was completed in a few seconds and the SHG intensity saturated.

It has been demonstrated that fs laser pulses can be employed to realize phase transition from disorder to order which is called laser-induced recrystallization.[42−44] In our case, the annealing of a-GaAs NSs is considered as a thermal process which occurs by the diffusion of atoms. The heat generated by the absorption of fs laser light increases the diffusion rate by providing the energy needed to break bonds. The movement of atoms has the effect of redistributing and eradicating the dislocations. In our case, the wavelength of the fs laser light was intentionally chosen to be close to the MD resonances of c-GaAs NSs. The linear and nonlinear absorption of the fs laser

DOI: 10.1021/acs.nanolett.7b01724
Nano Lett. XXXX, XXX, XXX−XXX

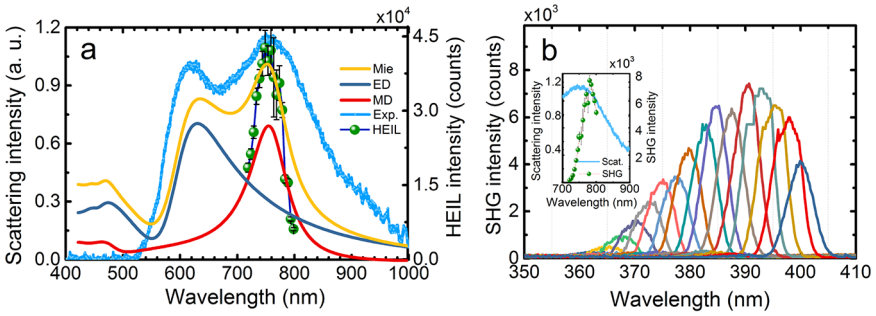

Figure 4. Enhanced HEIL and SHG at the MD resonances of GaAs NSs. (a) Excitation spectrum of the HEIL measured for a GaAs with $D \sim 190$ nm. The measured and calculated scattering spectra (including the ED and MD resonances) of the GaAs NS are also provided. (b) Spectra of the SHG measured for the GaAs NS at different excitation wavelengths. The excitation spectrum of the SHG together with the scattering spectrum are shown in the inset.

light increases rapidly with the emergence of the MD resonances, providing a positive feedback to the annealing process. As a result, a very low irradiance (~0.15 mJ/cm^2) was used for the annealing process as compared with the previous case.[27]

As shown in Figure 2b, up-converted luminescence began to appear in the nonlinear response spectra of GaAs NSs after annealing. This kind of luminescence is not easily observed because it requires that the radiative intraband transition time becomes comparable to the relaxation time of hot carriers which is 0.1−1.0 ps for GaAs.[13] Otherwise, only the down-converted luminescence resulting from the interband transition of electrons will be observed, similar to that observed in bulk GaAs which appears as a narrow spectrum peaking at the bandgap energy of GaAs (see the inset of Figure 3a). Previously, hot luminescence has been observed in Si nanowires coated with thin Ag films.[13] However, it originated from the phonon-assisted interband transition which is enhanced by plasmonic effect. It has been demonstrated that both the up- and down-converted luminescence emitted by the single hot spots on the surfaces of rough Au and Ag films belong to HEIL.[11] However, the energy states in the conduction band of metals below the Fermi level are filled by a large number of electrons which enable the population of the empty energy states above the Fermi level upon the pumping of the fs laser pulses. In our case, a significant enhancement in electric field is expected at the MD resonances of c-GaAs NSs after annealing (see SI S9). When a c-GaAs NS is resonantly excited at the MD resonance, electrons with very high density will be created in the conduction band through either single-photon-induced absorption or TPA (see SI S10). As shown in Figure 3a, efficient HEIL composed of up-and down-converted parts was generated through the intraband transition of hot electrons in the conduction band, quite similar to that observed in plasmonic hot spots.[11] It is remarkable that no luminescence peak was observed at the bandgap energy of GaAs (~1.42 eV), implying that the HEIL is governed by the intraband transition of hot electrons and the contribution of the interband transition is negligible due to the enhanced Auger recombination rate (see SI S11). It is also noticed that the peak of the HEIL is blue-shifted with increasing irradiance, which is quite similar to the blue-shift of blackbody radiation with increasing temperature.[11] We plotted the HEIL intensity as a function of the irradiance in a double-logarithmic coordinate and observed straight lines with different slopes for different energies of emitted photons (see the inset of Figure 3b). In Figure 3b, we show the dependence of the extracted slope on the energy of emitted photon which appears as a straight line going through the origin of the coordinate (see SI, Figure S12). This feature further confirms that the broadband luminescence emitted by c-GaAs NSs resonantly excited at their MD resonances originates from the intraband transition of hot electrons.[11]

To verify the enhanced radiative intraband transition rate, we also measured the lifetime of the HEIL at ~550 nm, as shown in Figure 3c. The decay of the HEIL can be fitted by using two exponential decay processes. The time constant for the fast and dominant decay process was derived to be ~82 ps, which is much faster than the luminescence lifetime of bulk GaAs at the bandgap energy (~490 ps). However, this value is still much longer than the relaxation time of hot electrons in c-GaAs (0.1−1.0 ps), implying that most hot electrons will relax rapidly to the bottom of the conduction band nonradiatively. Although the possibility of emitting photons has been enhanced significantly, it seems that highly efficient HEIL cannot be achieved for the radiative intraband transition lifetime of ~82 ps. In fact, it is expected that Auger recombination rate proportional to the third power of carrier density plays a crucial role as it will contribute to more hot electrons at high-energy states (see SI S11).[45] Thus, the rapid relaxation of hot electrons does not influence so much the HEIL.

To clarify the importance of the MD resonances in the generation of HEIL, we also examined the dependence of the HEIL intensity on the excitation wavelength for a c-GaAs NS, as shown in Figure 4a. It can be seen that the strongest HEIL was indeed generated at the MD resonance (~785 nm) of the GaAs NS where the maximum electric field enhancement is achieved, in good agreement with the predication based on the numerical simulation. For excitation wavelengths shorter or longer than the MD resonance, a rapid reduction in the HEIL intensity was observed. For example, the HEIL intensity generated by using an excitation wavelength of 800 nm was only about one-tenth of that generated resonantly at ~785 nm. It indicates that the MD resonances of GaAs NSs play a crucial role in the generation of HEIL. Apart from HEIL, enhanced SHG was also observed at the MD resonance, as shown in Figure 4b.

Physically, the HEIL of GaAs NSs originates from the high-temperature electron gas generated mainly by TPA when the MD resonances of GaAs NSs are resonantly excited. Since the energy of the excitation photons is larger than the bandgap energy of GaAs, the TPA process may involve either the sequential or the simultaneous absorption of two photons (see SI S10). Here, it should be emphasized that the momentum conservation requirement for the transition of electrons is

DOI: 10.1021/acs.nanolett.7b01724
Nano Lett. XXXX, XXX, XXX−XXX

greatly relaxed in GaAs NSs, similar to that in metallic nanoparticles.[11] In general, the pumping rate is much larger than the decay rate at the intermediate state. The HEIL intensity can be described by the following formula in which the enhancement at the wavelengths of both the absorption and the emission has been taken into account.[1,8,46]

$$I_{IL} = \eta(\lambda_{em})\delta(\lambda_{ex})\frac{1}{V^2}\int((E(\lambda_{ex}, r)/E_0)^4)dV \times \int((E(\lambda_{em}, r)/E_0)^2)dV \quad (1)$$

Here, $\eta(\lambda_{em})$ and $\delta(\lambda_{ex})$ are the quantum efficiency and TPA cross section of the GaAs NS, and $E(\lambda_{ex},r)/E_0$ and $E(\lambda_{em},r)/E_0$ denote the electric field enhancement factors at the excitation and emission wavelengths, respectively. The integrals run over the volume of the GaAs NS. In this work, we first simulated the electric field distributions for a c-GaAs NS with d = 200 nm at different wavelengths by using the FDTD method and then derived the enhancement factors at the corresponding wavelengths by using eq 1. From the spectra of the enhancement factors for the excitation and emission (see SI S13), it can be seen that the maximum enhancement factor of ∼40 for the excitation is achieved at the MD resonance of the GaAs NS (∼775 nm). In comparison, the enhancement factors in the range of 2−5 are observed in the wavelength range of 400−700 nm where the emission of the HEIL is observed. Therefore, a total enhancement of HEIL by 2 orders of magnitude is expected if we choose to excite the MD resonance of the GaAs NS, as we did in the experiments. Considering that the enhancement factor at the ED resonance of a core−shell GaAs NS is quite small (see SI S13), no obvious enhancement in the HEIL was observed at the photo energy corresponding to the ED resonance.

Concluding Remarks. In summary, we have successfully fabricated GaAs NSs and introduced the phase transition of crystal structure from amorphous or polycrystalline to monocrystalline by annealing GaAs NSs with fs laser pulses of a high repetition rate. Significantly enhanced electric and magnetic fields achieved at the MD resonances of c-GaAs NSs are exploited to generate a high-temperature electron gas which radiates broadband HEIL quite similar to blackbody radiation. Semiconductor NSs capable of emitting such kind of HEIL act as nanoscale incandescent light sources which is not limited by the bandgap energies of semiconductors. We believe that c-GaAs NSs with distinct ED and MD resonances will find potential applications in the construction of novel all-dielectric metamaterials and active photonic devices such as nanolasers.[47]

Methods. *Sample Preparation.* GaAs NSs with diameters ranging from 100 to 250 nm were fabricated by using laser-induced backward technique (see SI S1). A fs laser amplifier (Legend, Coherent) with a pulse duration of 100 fs and repetition rate of 1 kHz was employed in the ablation process. A 25 mm focal length objective was used to tightly focus the fs laser beam on a GaAs wafer with a spot diameter of ∼1 μm. GaAs NSs ejected from the GaAs wafer after the irradiation of fs laser light were collected by using a glass slide placed in front of the GaAs wafer. The morphology and crystallographic structure of the as-prepared GaAs NSs were examined by using SEM and high-resolution TEM, respectively.

Experimental Setup. The scattering spectra of GaAs NSs were measured by using dark-field microscopy (Observer A1, Zeiss). The annealing of GaAs NSs as well as the characterization of the nonlinear optical properties of GaAs NSs were carried out by using a fs laser oscillator with pulse duration of 130 fs and repetition rate of 76 MHz (Mira 900S, Coherent). The fs laser light was introduced into an inverted microscope and focused using a 100× objective on GaAs NSs. The nonlinear optical signals from GaAs NSs were collected by the same objective and directed to a spectrometer (SR500, Andor) for analysis. During the annealing process, the emission spectra of GaAs NSs were recorded at one second intervals.

Numerical Modeling. The scattering spectra of Si and GaAs NSs were calculated by using Mie theory or simulated by using the FDTD technique (commercial software developed by Lumerical Solution Inc. (http://www.lumerical.com).[48] In the FDTD simulation, a nonuniform mesh size with the smallest mesh size of 1 nm as well as a perfectly matched boundary condition was employed. The complex refractive indices for a-GaAs and c-GaAs used in the numerical simulations are provided in the SI (see SI S6).

■ ASSOCIATED CONTENT

Supporting Information

The Supporting Information is available free of charge on the ACS Publications website at DOI: 10.1021/acs.nanolett.7b01724.

Detailed sample preparation and microscopic characterization (PDF)

■ AUTHOR INFORMATION

Corresponding Author

*E-mail: slan@scnu.edu.cn.

ORCID

Jin Xiang: 0000-0003-0896-7526

Notes

The authors declare no competing financial interest.

■ ACKNOWLEDGMENTS

The authors would like to thank Prof. A. V. Gopal (Tata Institute of Fundamental Research, India) for fruitful discussion. S.L is thankful for the financial support from the National Key Research and Development Program of China (no. 2016YFA0201002). S.L., S.T., and Y.X. acknowledge the financial support from the National Nature and Science Foundation of China (grant nos. 11374109, 11674110, 11304047, and 11674130) and that from the Natural Science Foundation of Guangdong Province, China (grant nos. 2016A030308010, 2014A030313376, and 2016A030306016) and the Science and Technology Planning Project of Guangdong Province, China (grant no. 2015B090927006).

■ REFERENCES

(1) Viarbitskaya, S.; Teulle, A.; Marty, R.; Sharma, J.; Girard, C.; Arbouet, A.; Dujardin, E. *Nat. Mater.* **2013**, *12*, 426−432.
(2) Harutyunyan, H.; Martinson, A. B. F.; Rosenmann, D.; Khorashad, L. K.; Besteiro, L. V.; Govorov, A. O.; Wiederrecht, G. P. *Nat. Nanotechnol.* **2015**, *10*, 770−774.
(3) Borys, N. J.; Lupton, J. M. *J. Phys. Chem. C* **2011**, *115*, 13645−13659.
(4) Kleinman, S. L.; Frontiera, R. R.; Henry, A.-I.; Dieringer, J. A.; Van Duyne, R. P. *Phys. Chem. Chem. Phys.* **2013**, *15*, 21−36.
(5) Mohamed, M. B.; Volkov, V.; Link, S.; El-Sayed, M. A. *Chem. Phys. Lett.* **2000**, *317*, 517−523.
(6) Kabashin, A. V.; Evans, P.; Pastkovsky, S.; Hendren, W.; Wurtz, G. A.; Atkinson, R.; Pollard, R.; Podolskiy, V. A.; Zayats, A. V. *Nat. Mater.* **2009**, *8*, 867−871.

DOI: 10.1021/acs.nanolett.7b01724
Nano Lett. XXXX, XXX, XXX−XXX

(7) Zijlstra, P.; Chon, J. W. M.; Gu, M. *Nature* **2009**, *459*, 410−413.
(8) Chen, L.; Li, G. C.; Liu, G. Y.; Dai, Q. F.; Lan, S.; Tie, S. L.; Deng, H. D. *J. Phys. Chem. C* **2013**, *117*, 20146−20153.
(9) Boyd, G. T.; Yu, Z. H.; Shen, Y. R. *Phys. Rev. B: Condens. Matter Mater. Phys.* **1986**, *33*, 7923−7936.
(10) Zijlstra, P.; Orrit, M. *Rep. Prog. Phys.* **2011**, *74*, 106401.
(11) Haug, T.; Klemm, P.; Bange, S.; Lupton, J. M. *Phys. Rev. Lett.* **2015**, *115*, 067403.
(12) Zheng, Y.; Liu, H.; Xiang, J.; Dai, Q.; Ouyang, M.; Tie, S.; Lan, S. *Opt. Express* **2017**, *25*, 9262−9275.
(13) Cho, C.-H.; Aspetti, C. O.; Park, J.; Agarwal, R. *Nat. Photonics* **2013**, *7*, 285−289.
(14) Oulton, R. F.; Sorger, V. J.; Genov, D. A.; Pile, D. F. P.; Zhang, X. *Nat. Photonics* **2008**, *2*, 496−500.
(15) Oulton, R. F.; Sorger, V. J.; Zentgraf, T.; Ma, R.-M.; Gladden, C.; Dai, L.; Bartal, G.; Zhang, X. *Nature* **2009**, *461*, 629−632.
(16) Evlyukhin, A. B.; Novikov, S. M.; Zywietz, U.; Eriksen, R. L.; Reinhardt, C.; Bozhevolnyi, S. I.; Chichkov, B. N. *Nano Lett.* **2012**, *12*, 3749−3755.
(17) Kuznetsov, A. I.; Miroshnichenko, A. E.; Fu, Y. H.; Zhang, J.; Luk'yanchuk, B. *Sci. Rep.* **2012**, *2*, 492.
(18) Fu, Y. H.; Kuznetsov, A. I.; Miroshnichenko, A. E.; Yu, Y. F.; Luk'yanchuk, B. *Nat. Commun.* **2013**, *4*, 1527.
(19) Feng, T.; Xu, Y.; Zhang, W.; Miroshnichenko, A. E. *Phys. Rev. Lett.* **2017**, *118*, 173901.
(20) Grinblat, G.; Li, Y.; Nielsen, M. P.; Oulton, R. F.; Maier, S. A. *ACS Nano* **2017**, *11*, 953−960.
(21) Ginn, J. C.; Brener, I.; Peters, D. W.; Wendt, J. R.; Stevens, J. O.; Hines, P. F.; Basilio, L. I.; Warne, L. K.; Ihlefeld, J. F.; Clem, P. G.; Sinclair, M. B. *Phys. Rev. Lett.* **2012**, *108*, 097402.
(22) Person, S.; Jain, M.; Lapin, Z.; Saenz, J. J.; Wicks, G.; Novotny, L. *Nano Lett.* **2013**, *13*, 1806−1809.
(23) Zhao, Q.; Zhou, J.; Zhang, F.; Lippens, D. *Mater. Today* **2009**, *12*, 60−69.
(24) Kuznetsov, A. I.; Miroshnichenko, A. E.; Brongersma, M. L.; Kivshar, Y. S.; Luk'yanchuk, B. *Science* **2016**, *354*, 2472.
(25) Xiang, J.; Li, J.; Li, H.; Zhang, C.; Dai, Q.; Tie, S.; Lan, S. *Opt. Express* **2016**, *24*, 11420−11434.
(26) Zywietz, U.; Reinhardt, C.; Evlyukhin, A. B.; Birr, T.; Chichkov, B. N. *Appl. Phys. A: Mater. Sci. Process.* **2014**, *114*, 45−50.
(27) Zywietz, U.; Evlyukhin, A. B.; Reinhardt, C.; Chichkov, B. N. *Nat. Commun.* **2014**, *5*, 3402.
(28) Bakker, R. M.; Permyakov, D.; Yu, Y. F.; Markovich, D.; Paniagua-Dominguez, R.; Gonzaga, L.; Samusev, A.; Kivshar, Y.; Luk'yanchuk, B.; Kuznetsov, A. I. *Nano Lett.* **2015**, *15*, 2137−2142.
(29) Shcherbakov, M. R.; Neshev, D. N.; Hopkins, B.; Shorokhov, A. S.; Staude, I.; Melik-Gaykazyan, E. V.; Decker, M.; Ezhov, A. A.; Miroshnichenko, A. E.; Brener, I.; Fedyanin, A. A.; Kivshar, Y. S. *Nano Lett.* **2014**, *14*, 6488−6492.
(30) Shcherbakov, M. R.; Shorokhov, A. S.; Neshev, D. N.; Hopkins, B.; Staude, I.; Melik-Gaykazyan, E. V.; Ezhov, A. A.; Miroshnichenko, A. E.; Brener, I.; Fedyanin, A. A.; Kivshar, Y. S. *ACS Photonics* **2015**, *2*, 578−582.
(31) Shcherbakov, M. R.; Vabishchevich, P. P.; Shorokhov, A. S.; Chong, K. E.; Choi, D.-Y.; Staude, I.; Miroshnichenko, A. E.; Neshev, D. N.; Fedyanin, A. A.; Kivshar, Y. S. *Nano Lett.* **2015**, *15*, 6985−6990.
(32) Zhang, C.; Xu, Y.; Liu, J.; Li, J.; Xiang, J.; Li, H.; Lan, S.; Miroshnichenko, A. E. *arXiv*:1703.10287, **2017**.
(33) Moitra, P.; Yang, Y.; Anderson, Z.; Kravchenko, I. I.; Briggs, D. P.; Valentine, J. *Nat. Photonics* **2013**, *7*, 791−795.
(34) Gili, V. F.; Carletti, L.; Locatelli, A.; Rocco, D.; Finazzi, M.; Ghirardini, L.; Favero, I.; Gomez, C.; Lemaitre, A.; Celebrano, M.; De Angelis, C.; Leo, G. *Opt. Express* **2016**, *24*, 15965−15971.
(35) Liu, S.; Sinclair, M. B.; Saravi, S.; Keeler, G. A.; Yang, Y.; Reno, J.; Peake, G. M.; Setzpfandt, F.; Staude, I.; Pertsch, T.; Brener, I. *Nano Lett.* **2016**, *16*, 5426−5432.
(36) Shcherbakov, M. R.; Liu, S.; Zubyuk, V. V.; Vaskin, A.; Vabishchevich, P. P.; Keeler, G.; Pertsch, T.; Dolgova, T. V.; Staude, I.; Brener, I.; Fedyanin, A. A. *Nat. Commun.* **2017**, *8*, 17.
(37) Adachi, S. *Optical constants of crystalline and amorphous semiconductors: numerical data and graphical information*; Springer Science & Business Media, 1999.
(38) Palik, E. D. *Handbook of optical constants of solids*; Academic Press, 1998.
(39) Saeta, P.; Wang, J. K.; Siegal, Y.; Bloembergen, N.; Mazur, E. *Phys. Rev. Lett.* **1991**, *67*, 1023−1026.
(40) Sokolowski-Tinten, K.; Bialkowski, J.; Boing, M.; Cavalleri, A.; von der Linde, D. *Phys. Rev. B: Condens. Matter Mater. Phys.* **1998**, *58*, 11805−11808.
(41) Ganeev, R. A.; Ryasnyanskiy, A. I.; Usmanov, T. *Opt. Commun.* **2007**, *272*, 242−246.
(42) Campisano, S. U.; Foti, G.; Rimini, E.; Eisen, F. H.; Tseng, W. F.; Nicolet, M. A.; Tandon, J. L. *J. Appl. Phys.* **1980**, *51*, 295−298.
(43) Vitali, G.; Zollo, G.; Pizzuto, C.; Manno, D.; Kalitzova, M.; Rossi, M. *Appl. Phys. Lett.* **1996**, *69*, 4072−4074.
(44) Shieh, J.-M.; Chen, Z.-H.; Dai, B.-T.; Wang, Y.-C.; Zaitsev, A.; Pan, C.-L. *Appl. Phys. Lett.* **2004**, *85*, 1232−1234.
(45) Li, S. S. *Semiconductor physical electronics*; Springer, 2012; Chapter 6.
(46) Ghenuche, P.; Cherukulappurath, S.; Taminiau, T. H.; van Hulst, N. F.; Quidant, R. *Phys. Rev. Lett.* **2008**, *101*, 116805.
(47) Saxena, D.; Mokkapati, S.; Parkinson, P.; Jiang, N.; Gao, Q.; Tan, H. H.; Jagadish, C. *Nat. Photonics* **2013**, *7*, 963−968.
(48) A commercial software developed by Lumerical Solutions Inc. (https://www.lumerical.com) is used for the numerical simulations.

DOI: 10.1021/acs.nanolett.7b01724
Nano Lett. XXXX, XXX, XXX−XXX